communications biology

Article

https://doi.org/10.1038/s42003-024-06866-3

Low frequency sinusoidal electromagnetic fields promote the osteogenic differentiation of rat bone marrow mesenchymal stem cells by modulating miR-34b-5p/STAC2

Xuan Fang[1,6], Changyu Liu[1,6], Kang Wei[1], Zixing Shu[1], Yi Zou[1], Zihao Zhang[2], Qing Ding[3], Shaoze Jing[4], Weigang Li[3], Tianqi Wang[5], Hao Li[1], Hua Wu[1], Chaoxu Liu[1] ✉ & Tian Ma[1] ✉

Electromagnetic fields (EMFs) have emerged as an effective treatment for osteoporosis. However, the specific mechanism underlying their therapeutic efficacy remains controversial. Herein, we confirm the pro-osteogenic effects of 15 Hz and 0.4-1 mT low-frequency sinusoidal EMFs (SEMFs) on rat bone marrow mesenchymal stem cells (BMSCs). Subsequent miRNA sequencing reveal that miR-34b-5p is downregulated in both the 0.4 mT and 1 mT SEMFs-stimulated groups. To clarify the role of miR-34b-5p in osteogenesis, BMSCs are transfected separately with miR-34b-5p mimic and inhibitor. The results indicate that miR-34b-5p mimic transfection suppress osteogenic differentiation, whereas inhibition of miR-34b-5p promote osteogenic differentiation of BMSCs. In vivo assessments using microcomputed tomography, H&E staining, and Masson staining show that miR-34b-5p inhibitor injections alleviate bone mass loss and trabecular microstructure deterioration in ovariectomy (OVX) rats. Further validation demonstrates that miR-34b-5p exerts its effects by regulating *STAC2* expression. Modulating the miR-34b-5p/*STAC2* axis attenuate the pro-osteogenic effects of low-frequency SEMFs on BMSCs. These studies indicate that the pro-osteogenic effect of SEMFs is partly due to the regulation of the miR-34b-5p/*STAC2* pathway, which provides a potential therapeutic candidate for osteoporosis.

Postmenopausal osteoporosis is a metabolic bone disease that causes bone fragility and increases the risk of fractures[1]. The imbalance between bone resorption and bone formation plays a pivotal role in osteoporosis[2]. Consequently, pharmacological interventions targeting bone remodeling, such as bisphosphonates, constitute the primary therapeutic approach for managing osteoporosis[3]. However, the utilization of bisphosphonate compounds may be constrained in some patients due to severe adverse effects[4]. In recent years, stem cell-based therapy has emerged as a promising approach for the treatment of various diseases[5]. Within this realm, bone marrow mesenchymal stem cells (BMSCs) have garnered attention due to their pluripotent nature and substantial potential for osteogenic differentiation[6]. Numerous studies have underscored the beneficial effects of harnessing the osteogenic capacity of BMSCs in treating osteoporosis[7–9]. Nevertheless, further investigation is still required on how to effectively promote the osteogenic differentiation of BMSCs.

Over the past few decades, electromagnetic fields (EMFs) have received increasing attention in the treatment of skeletal diseases as a safe, effective, and non-invasive therapy method[10–12]. One of the key mechanisms driving

[1]Department of Orthopedics, Tongji Hospital, Tongji Medical College, Huazhong University of Science and Technology, Wuhan, China. [2]Division of Cardiovascular Surgery, Tongji Hospital, Tongji Medical College, Huazhong University of Science and Technology, Wuhan, China. [3]Department of Pediatric Surgery, Tongji Hospital, Tongji Medical College, Huazhong University of Science and Technology, Wuhan, China. [4]Department of Orthopedics, Shanxi Bethune Hospital, Shanxi Medical University, Taiyuan, China. [5]Departments of Orthopaedic Surgery, Yong Loo Lin School of Medicine, National University of Singapore, Singapore, Singapore. [6]These authors contributed equally: Xuan Fang, Changyu Liu. ✉e-mail: chaoxuliu@hotmail.com; 2020TJ5151@hust.edu.cn

this therapeutic potential is the capacity of EMFs, when applied at specific intensities and frequencies, to influence the fate of stem cells, thereby promoting osteogenesis, chondrogenesis and angiogenesis[13]. The optimal therapeutic effect of EMFs for skeletal disorders is observed within the frequency range of 15–30 Hz, as bone cells demonstrate a high degree of selectivity towards this range[14]. Consequently, some studies have employed low-frequency EMFs to assist in the MSCs-loading tissue engineering techniques, aiming to achieving bone repair and regeneration by enhancing bone formation[15–17]. Nevertheless, the optimal intensity range for EMFs treatment and the precise mechanism by which EMFs facilitate the osteogenic differentiation of BMSCs remain to be thoroughly understood.

MicroRNAs (miRNAs) are a group of non-coding RNAs that consist of ~22 nucleotides[18]. They have been shown to play crucial roles as post-transcriptional regulators in cellular development, differentiation, and disease progression[19]. Furthermore, several miRNAs, such as miR-148b, miR-26 and miR-196a, have been identified as key regulators of promoting osteogenic induction in stem cells[18,20]. As a physical stimulus, EMFs have been reported to influence the expression of a variety of miRNAs[21,22]. For instance, exposure to EMFs has been shown to increase the expression of miR-144 and miR-375 in gastric cancer cells[23]. Additionally, EMFs at specific frequencies could reduce the expression of exosomal miR-1246, resulting in angiogenesis inhibition[24]. While the use of EMF-regulated miRNAs to enhance BMSCs osteogenic differentiation has garnered attention[21], the specific miRNAs involved, and their related mechanisms remain unclear.

Recent studies have suggested that EMF-induced calcium ion oscillations, triggered by the activation of calcium ion channels, may play a significant role in determining the differentiation of BMSCs[14,25]. The elevated calcium ions initiate downstream molecules and various calcium-sensitive signaling cascades, which in turn influence cell differentiation, proliferation, and metabolism[26,27]. Meanwhile, some miRNAs have been identified to regulate calcium channels and influence transmembrane calcium transport, such as miR-21-5p[28] and miR-27a[29]. Nevertheless, the role of EMF-regulated miRNAs in the regulation of calcium channels remains to be elucidated.

In this study, the effect of sinusoidal EMFs (SEMFs) at 15 Hz combined with different magnetic field intensities on promoting osteogenic differentiation of BMSCs was further explored, based on our previous studies on the parameters of low-frequency SEMFs[15,30]. Subsequently, miRNA sequencing revealed that exposure to 15 Hz SEMFs at 0.4 mT and 1 mT significantly decreased the expression of miR-34b-5p. The role of miR-34b-5p in SEMFs-induced osteogenic differentiation in vitro was then investigated. Meanwhile, the therapeutic efficacy of regulating miR-34b-5p on osteoporosis in ovariectomy (OVX) rats was also assessed. At last, we demonstrated that miR-34b-5p and calcium channel-related gene SH3 and cysteine-rich domain 2 (*STAC2*) are involved in SEMFs-mediated osteogenesis. In summary, the present study explored the mechanisms underlying the pro-osteogenic effects of SEMFs and suggested a potential therapeutic target for osteoporosis.

Results

SEMFs with a frequency of 15 Hz and intensities between 0.4 and 1 mT promoted osteogenic differentiation of BMSCs

In the presence of osteogenic medium (OM), rat BMSCs were exposed to SEMFs at a frequency of 15 Hz and varying magnetic field intensities (0.4, 0.7, or 1 mT) for either 7 or 14 days. The effects of SEMFs on osteogenic differentiation were assessed using Western blot, RT-qPCR, ALP, and ARS staining assays (Fig. 1a). The results revealed a significant increase in ARS staining intensity following exposure to SEMFs at all tested intensities, with the most pronounced increase observed under 0.4 mT SEMF stimulation (Fig. 1b, c). Consistent with these findings, ALP staining also demonstrated increased activity, with the deepest staining detected under 1 mT SEMF exposure (Fig. 1b, c). RT-qPCR analysis demonstrated a significant upregulation in the relative expression levels of osteogenic markers (*ALP, RUNX2, BMP2, OCN,* and *OPN*) (Fig. 1d). Moreover, protein expression levels of osteogenic makers, including Active-β-catenin, RUNX2, and ALP, were elevated upon SEMFs exposure at 0.4 mT, 0.7 mT, and 1 mT (Fig. 1e, f). These findings indicate that BSMCs exposed to low-frequency SEMFs ranging from 0.4 to 1 mT exhibit enhanced potential for osteogenic differentiation. Based on these results, SEMFs at 0.4 mT and 1 mT were selected for further investigation regarding their effects on osteogenic differentiation.

Low-frequency SEMFs regulated miRNAs expression in BMSCs

To explore the regulatory effects of low-frequency SEMFs on miRNA expression in osteogenic differentiation, BMSCs were continuously exposed to 15 Hz SEMFs at intensities of either 0.4 mT or 1 mT for 7 days under OM. Subsequently, miRNAs from the control, 0.4 mT, and 1 mT groups were collected for sequencing. The results revealed differential expression of 98 miRNAs during SEMFs stimulation at 0.4 mT, with 64 miRNAs upregulated and 34 down-regulated (Fig. 2a, Supplementary Data 1). At an intensity of 1 mT, 46 miRNAs exhibited elevated expression, while 37 showed down-regulation (Fig. 2b, Supplementary Data 2). The Venn diagram and heatmap depicted 26 miRNAs co-regulated in both the 0.4 mT group and the 1 mT group compared to the control group, with 17 upregulated and 9 down-regulated (Fig. 2c, d, Supplementary Data 3). Based on the miRNA sequencing data, the top 5 commonly differentially expressed miRNAs were selected for further validation of their expression levels utilizing RT-qPCR. As shown in Fig. 2e, the expression of miR-7a-5p, miR-27a-5p, miR-984, and miR-129-5p was significantly upregulated after SEMFs stimulation while the expression of miR-34b-5p decreased. Considering that miRNAs generally function as negative regulators[19], the impact of miR-34b-5p on osteogenic differentiation was further investigated in subsequent studies.

miR-34b-5p expression affected the osteogenic differentiation of BMSCs

To investigate the biological effects of miR-34b-5p during osteogenic induction, BMSCs were transfected with either miR-34b mimic or miR-34b-5p inhibitor. As depicted in Supplementary Fig. 1a, the transfection efficiency was low at a concentration of 20 nM but reached comparability at higher concentrations of 50 nM and 100 nM. Consequently, 50 nM was chosen as the optimal transfection concentration. RT-qPCR results illustrated significant upregulation or downregulation of miR-34b-5p expression following transfection with either the mimic or inhibitor (Supplementary Fig. 1b). Next, the impact of modulating miR-34b-5p on cell proliferation was assessed via EdU assay. The results indicated that transfection with the miR-34b-5p mimic inhibited cell proliferation, while transfection with the miR-34b-5p inhibitor promoted BMSCs growth (Fig. 3a, b). ARS and ALP staining results indicated that increasing miR-34b-5p expression attenuated mineralization and ALP activity induced by OM, whereas inhibiting miR-34b-5p enhanced ALP activity and formation of mineralized calcium nodules (Fig. 3c, d). Furthermore, the mRNA levels of *OPN, ALP,* and *OCN* were decreased in miR-34b-5p mimic group, while exhibiting an increase in the miR-34b-5p inhibitor group (Fig. 3e). Western blot results also indicated that transfection of miR-34b-5p mimic decreased the protein levels of Active-β-Catenin and RUNX2, whereas miR-34b-5p inhibitor transfection accentuated the expressions of β-Catenin, Active-β-Catenin, RUNX2, and ALP (Fig. 3f, g).

miR-34b-5p inhibitor alleviated osteoporosis in OVX models

The pro-osteogenic function of regulating miR-34b-5p expression was investigated in an in vivo rat model with OVX-induced osteoporosis. Rats in the OVX+miR-34b-5p inhibitor group received miR-34b-5p inhibitor injections every 2 weeks for a total of 10 weeks (Fig. 4a, b). Micro-CT scanning and 3D reconstruction revealed a reduction in bone mass and impaired trabecular microstructure in the OVX group, while inhibition of miR-34b-5p partially ameliorated these detrimental effects (Fig. 4c). Subsequent analysis of bone morphometric parameters further supported these findings, demonstrating that regular injections of miR-34b-5p reversed the decline of BV/TV, TB.N, and TB.Th, and attenuated the increase in TB.Sp

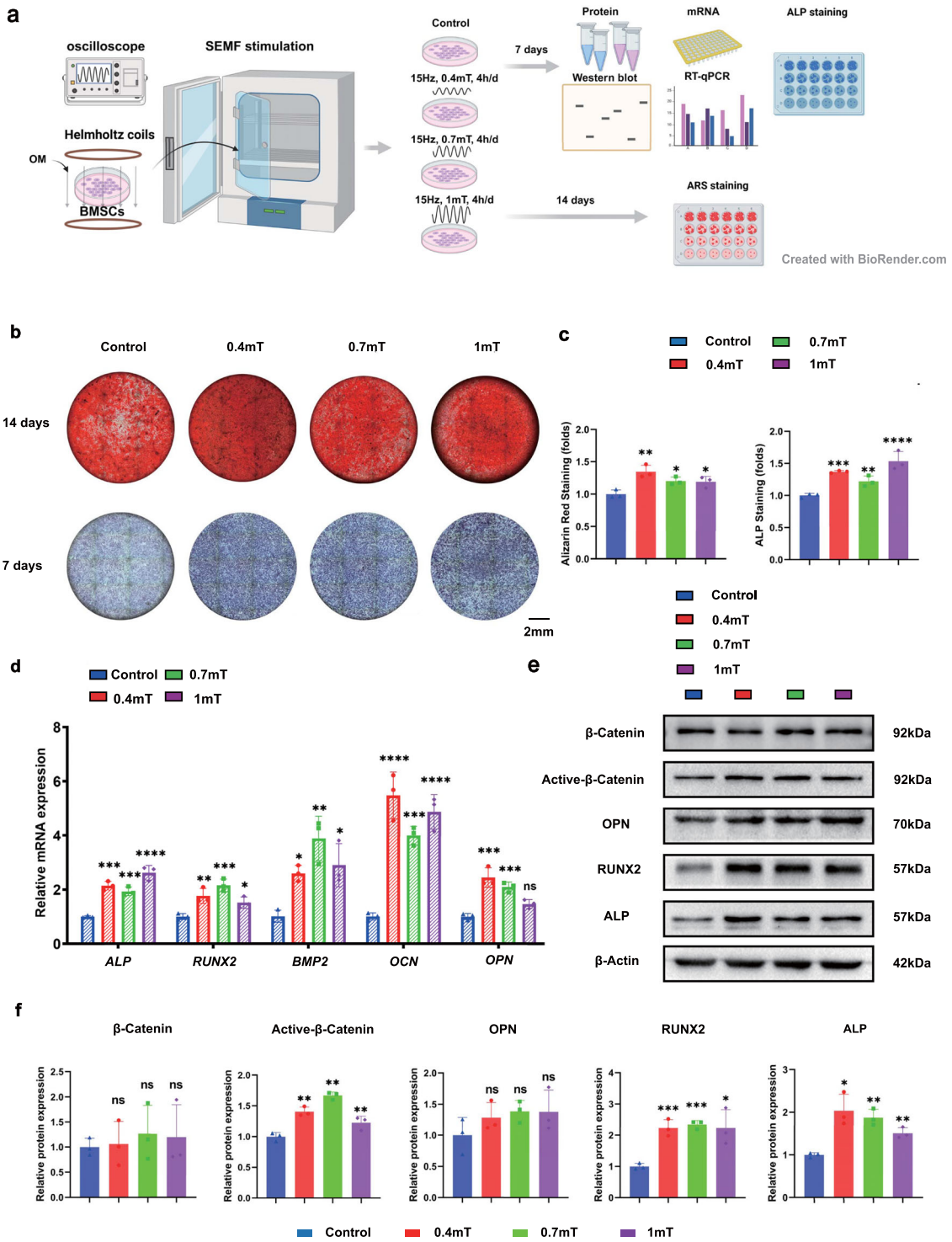

Fig. 1 | SEMFs with a frequency of 15 Hz and intensities between 0.4 and 1 mT promoted osteogenic differentiation of BMSCs. a Schematic diagram showing the assessment of SEMFs' impact on osteogenic differentiation. **b** ALP and ARS staining assays of BMSCs exposed to SEMFs at varying magnetic field intensities. **c** Semi-quantitative analyses of ALP and ARS staining intensities. **d** RT-qPCR results depicting the expression levels of osteogenic genes (*ALP, RUNX2, BMP2, OCN, OPN*) in BMSCs cultured in OM for 7 days and exposed to SEMFs at different magnetic field intensities. **e** Western blot results showing the protein levels of osteogenic markers (β-catenin, Active-β-catenin, OPN, RUNX2, and ALP) in BMSCs cultured in OM for 7 days and exposed to SEMFs at different magnetic field intensities. **f** Quantitative analysis of osteogenic protein expression. Data are presented as mean ± SD; N = 3/group; $^{*}p < 0.05$; $^{**}p < 0.01$; $^{***}p < 0.001$; $^{****}p < 0.0001$; ns, not significant by one-way ANOVA.

induced by OVX (Fig. 4d–g). Following this, H&E and Masson staining were conducted to assess the histomorphological differences among three groups. Decreased trabecular bone mass was observed in OVX group; however, the bone loss induced by OVX was markedly alleviated after treatment with miR-34b-5p inhibitor (Fig. 5a, b).

miR-34b-5p modulated *STAC2* expression

To further elucidate the mechanisms by which low-frequency SEMFs promote osteogenesis and the target genes regulated by miR-34b-5p, total RNA was extracted from the control, 0.4 mT-stimulated, and 1 mT-stimulated groups for RNA sequencing. In the 0.4 mT group, 557 genes were

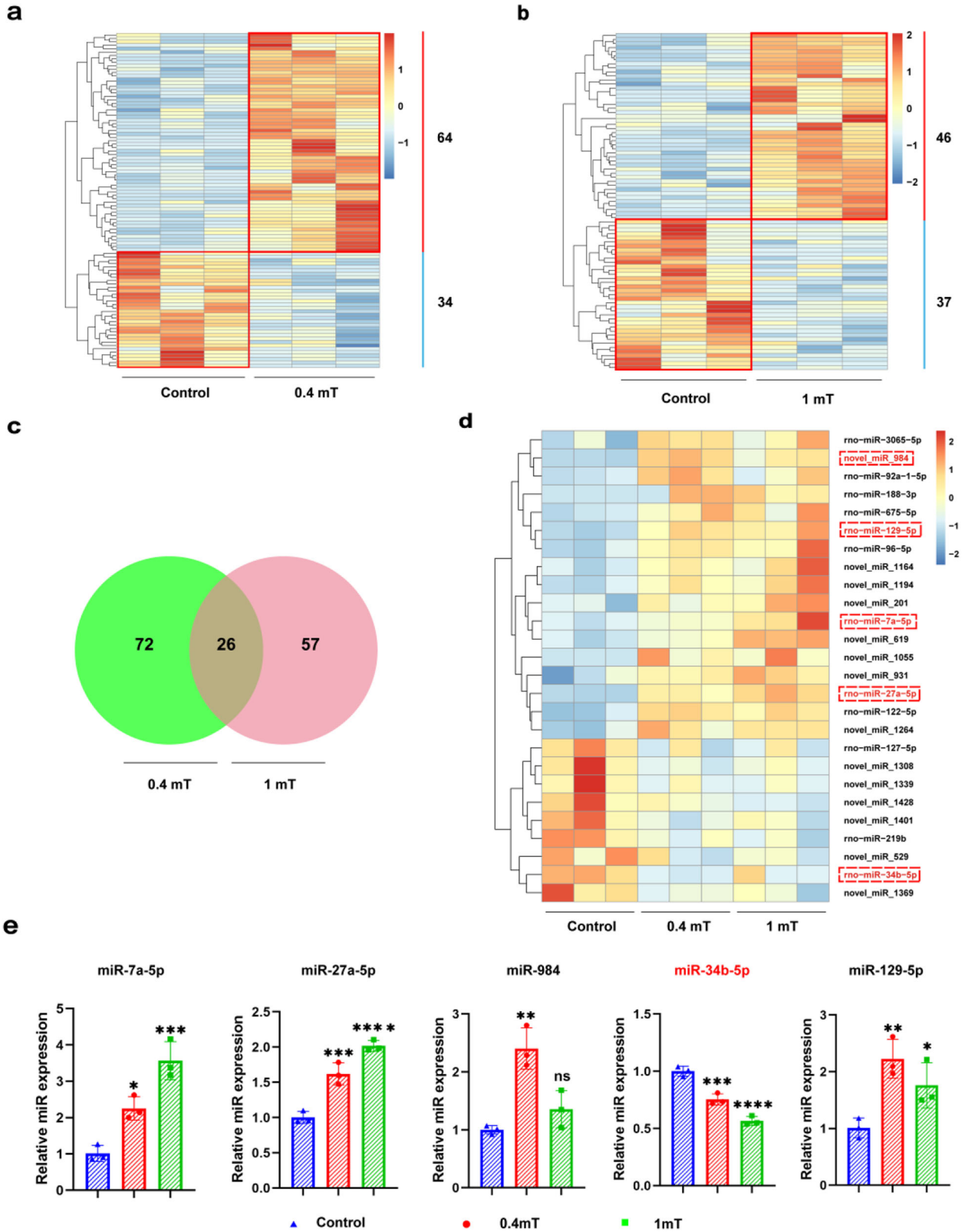

Fig. 2 | Low-frequency SEMFs regulated miRNAs expression in BMSCs. **a**, **b** Heatmaps depicting changes in miRNAs expression within BMSCs stimulated with 0.4 mT or 1 mT SEMFs. **c** A Venn diagram illustrating the intersection of differential miRNAs after stimulation with 0.4 mT or 1 mT low-frequency SEMFs. **d** A heatmap displaying the 26 commonly differentially expressed miRNAs. **e** The relative expressions of miR-7a-5p, miR-27a-5p, miR-984, miR-34b-5p and miR-129-5p after exposure to 0.4 mT or 1 mT SEMFs. Data are presented as mean ± SD; N = 3/group; *$p < 0.05$; **$p < 0.01$; ***$p < 0.001$; ****$p < 0.0001$; ns, not significant by one-way ANOVA.

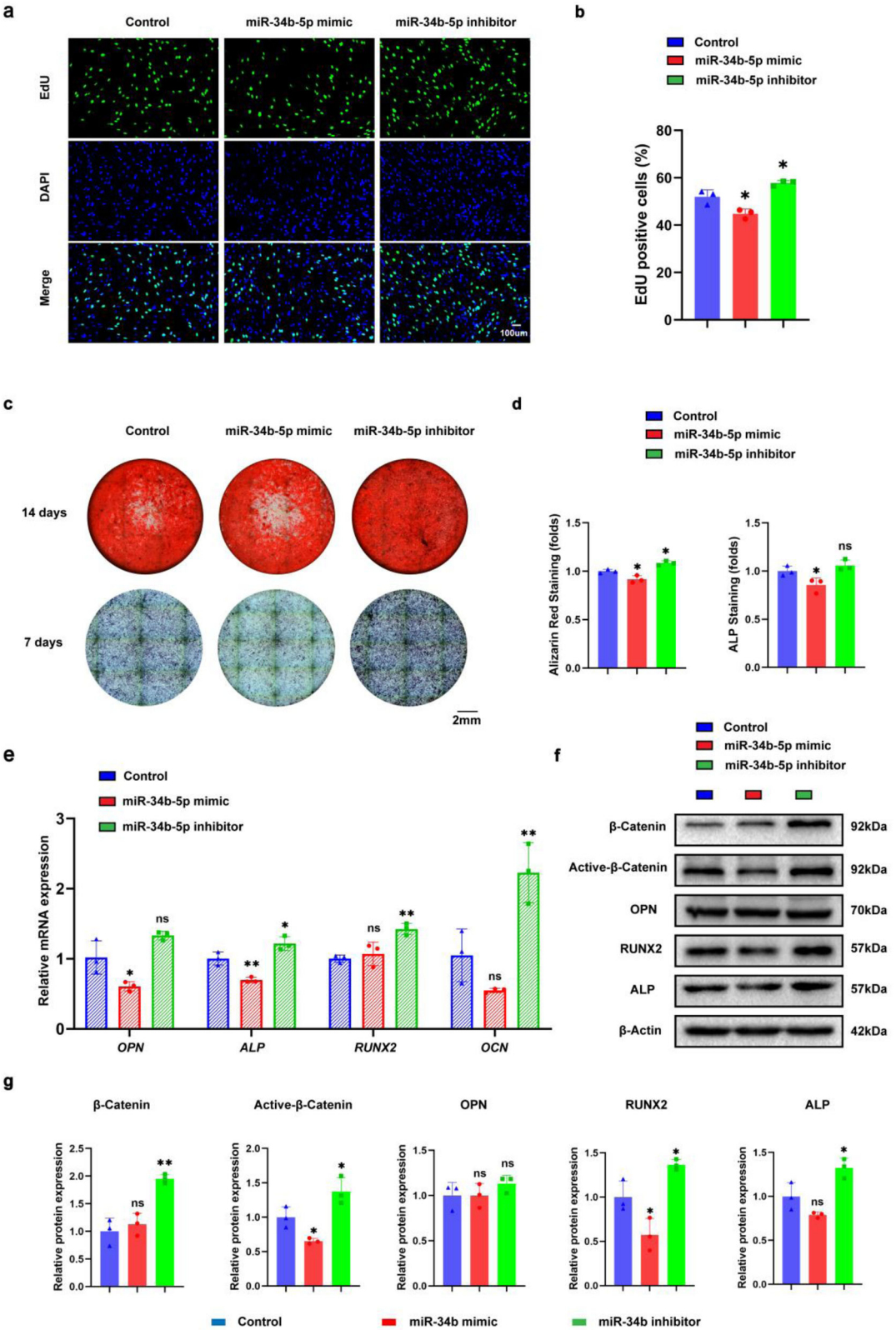

Fig. 3 | miR-34b-5p expression affected the osteogenic differentiation of BMSCs. **a** The proliferation of BMSCs after transfected with miR-34b-5p mimic or inhibitor was assessed by EdU assay. **b** Quantitative analysis of EdU assay. **c** ALP and ARS staining assays of BMSCs transfected with miR-34b-5p mimic or inhibitor. **d** Semi-quantitative analyses of ALP and ARS staining intensities. The quantitative analyses of staining intensities were normalized based on changes in cell number resulting from the modulation of miR-34b-5p activity. **e** The results of the RT-qPCR showing the expression levels of osteogenic genes following a 7-day transfection of miR-34b-5p mimic or inhibitor (*OPN*, *ALP*, *RUNX2*, *OCN*). **f** The results of the western blots showing the protein levels of osteogenic makers (β-catenin, Active-β-catenin, OPN, RUNX2, and ALP) after 7-day transfection of miR-34b-5p mimic or inhibitor. **g** Quantitative analysis of osteogenic protein expression. Data represent mean ± SD; N = 3/group; $^{*}p < 0.05$; $^{**}p < 0.01$; ns, not significant by one-way ANOVA.

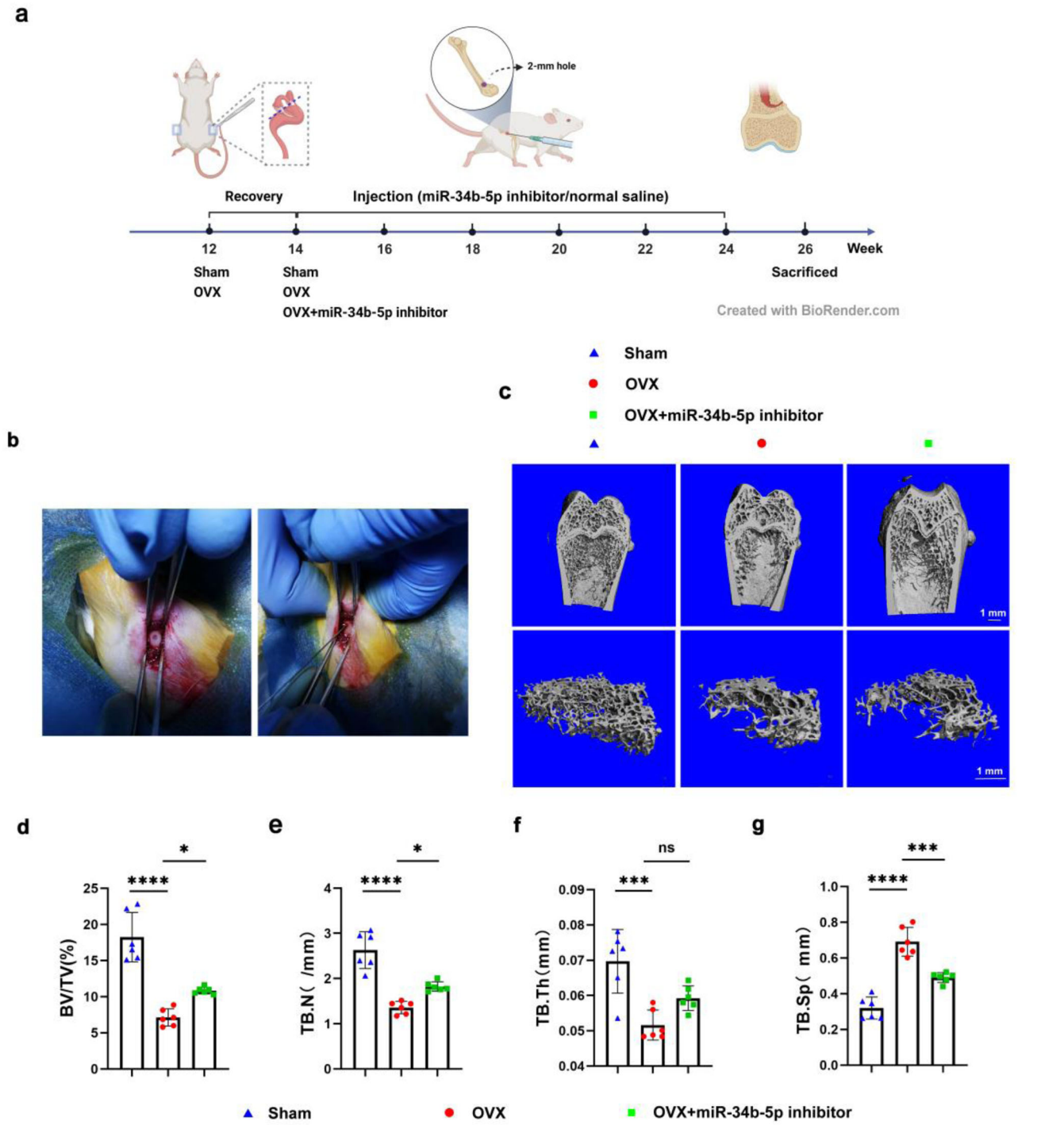

Fig. 4 | miR-34b-5p inhibitor alleviated osteoporosis in OVX models. a Rats flow chart of injecting miR-34b-5p inhibitor against osteoporosis. **b** Intraoperative picture of injection of miR-34b-5p inhibitor. **c** Representative micro-CT images of the femurs in each group. Scale bar = 1 mm. **d**–**g** Micro-CT parameters of BV/TV, TB.N, TB.Th and TB.Sp in each group. Data represent mean ± SD; N = 6/group; $^{*}p < 0.05$; $^{***}p < 0.001$; $^{****}p < 0.0001$; ns, not significant by one-way ANOVA.

upregulated and 530 genes were downregulated compared to the control (Fig. 6a). After stimulation with 1 mT SEMFs, 566 genes were upregulated and 516 genes were downregulated (Fig. 6b). Subsequently, the genes commonly regulated under stimulation with these two different magnetic field intensities were intersected, and GO enrichment analysis was conducted (Fig. 6c, d). Notably, ion transport, especially calcium ion transport, were significantly upregulated after SEMFs stimulation (Fig. 6d), aligning with previous studies[31–34]. Therefore, we sought to explore the relationship between SEMFs-regulated miRNAs and calcium ion transport by intersecting genes related to calcium ion transport in the GO database with predicted target genes of miR-34b-5p in the Targetscan database, identifying *STAC2* and *PLCG1* (Fig. 6e). Given that the Total Context score (indicating targeting probability[19]) of *STAC2* was markedly higher than that of *PLCG1* (Supplementary Data 4), *STAC2* was selected for further investigation regarding its interaction with miR-34b-5p. Dual-luciferase reporter assays were employed to confirm miR-34b-5p's interaction with *STAC2* (Fig. 6f, g). Transfection of miR-34b-5p mimic reduced luciferase activity compared to the control mimic, while transfection of miR-34b-5p inhibitor increased luciferase activity (Fig. 6g). Experimental validation showed that STAC2 protein expression was up-regulated in BMSCs treated with low-frequency

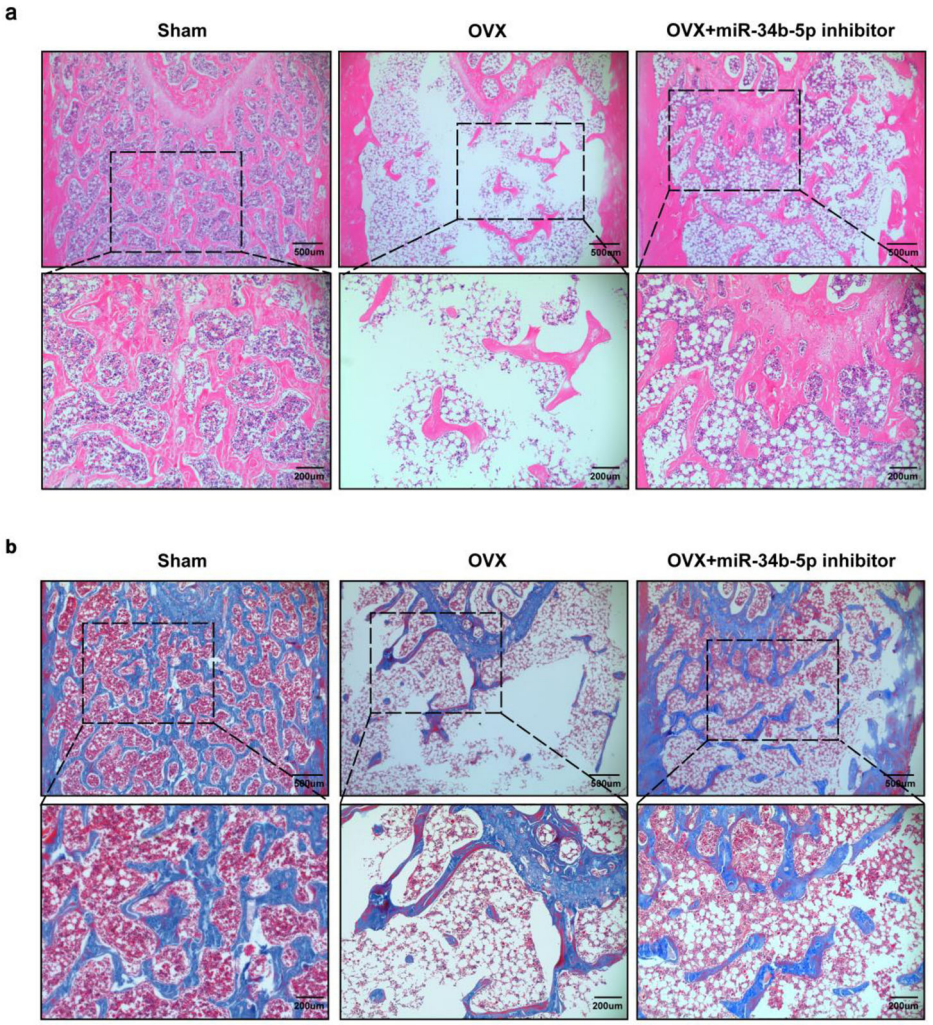

Fig. 5 | miR-34b-5p inhibitor alleviated osteoporosis in OVX models. a Representative image of H&E staining in each group showing the bone volume and new bone formation. **b** Representative images of Masson staining in each group showing the bone volume and new bone formation.

SEMF (15 Hz, 0.4–1 mT) for 2 weeks (Fig. 6h). Subsequent transfection of miR-34b-5p mimic and inhibitor into BMSCs altered STAC2 protein level accordingly (Fig. 6i).

Low-frequency SEMFs promoted osteogenic differentiation of BMSCs by regulating the miR-34b-5p/*STAC2* axis

To further investigate the role of the miR-34b-5p/*STAC2* pathway in promoting osteogenesis under SEMF stimulation, miR-34b-5p mimic, and *STAC2* siRNA were separately transfected into BMSCs every 4 days while being exposed to 0.4 mT low-frequency SEMFs for 7 or 14 days. ARS staining and ALP staining assay revealed a significant decrease in calcium nodules and ALP activity in the miR-34b-5p mimic and *STAC2* siRNA transfected groups compared with the SEMFs-stimulated group (Fig. 7a, b). At the mRNA level, *BMP2, ALP, RUNX2*, and *OCN* were observed to be down-regulated (Fig. 7c). At the protein level, transfection of miR-34b-5p mimic attenuated the SEMF-induced upregulation of STAC2, and both of transfections significantly reversed the increase of osteogenic makers induced by SEMFs (Fig. 7d, e). These results indicate that the pro-osteogenic effects of SEMFs are partially attributable to modulating miR-34b-5p/*STAC2* axis.

Discussion

This study aimed to investigate the potential of 0.4–1 mT low-frequency SEMFs to stimulate osteogenic differentiation of BMSCs. We identified miR-34b-5p, one of the top 5 differentially expressed miRNAs during this process, as a key regulator in osteogenic differentiation. Subsequently, miR-34b-5p was regulated in vitro to verify its regulatory role in osteogenesis. In vivo experiments with miR-34b-5p inhibitor injections ameliorated OVX-induced bone loss and trabecular structure deterioration. Combined with transcriptome sequencing analysis, an increase in calcium ion transport activity was observed after SEMF stimulation, and *STAC2* was identified in the Targetscan database as a target gene of miR-34b-5p. Finally, targeting the miR-34b-5p/*STAC2* axis attenuated the osteogenic effect of SEMFs.

Despite advancements in promoting osteogenesis and decreasing bone loss through EMF therapy, identifying the appropriate therapeutic EMF parameters (intensity, frequency and stimulation time) remains challenging due to their complexity. Ferronoi et al. utilized 1 mT and 50 Hz pulsed EMF (PEMF) to stimulate MSCs for 6 h/d to promote proliferation and osteogenic differentiation[35]. Other studies demonstrated that PEMFs interventions at 1.8 mT and 15 Hz, 2.4 mT and 15 Hz, 1 mT, and 26 Hz also exhibited the potential to contribute to osteogenic differentiation[36,37]. In addition, a significant osteogenic effect was observed under the continuous stimulation of 0.1 mT and 50 Hz PEMFs[38]. For the parameters selection of SEMFs, previous studies have concentrated on examining the biological effects of 15–75 Hz, 0.3–2.4 mT SEMFs[39–42]. Zhou et al. demonstrated that 50 Hz was the optimal frequency for osteogenic differentiation in 0–100 Hz SEMFs. At this frequency, 1.8 mT was identified as the optimal intensity to promote osteogenic differentiation and mineralization[42]. The results obtained in this study confirmed the pro-osteogenic effects of 15 Hz SEMFs, with more pronounced effects observed at 0.4 mT and 1 mT.

In the skeletal system, miRNAs modulate osteoblast-related developmental signals and osteoclast-mediated bone resorption by inhibiting the

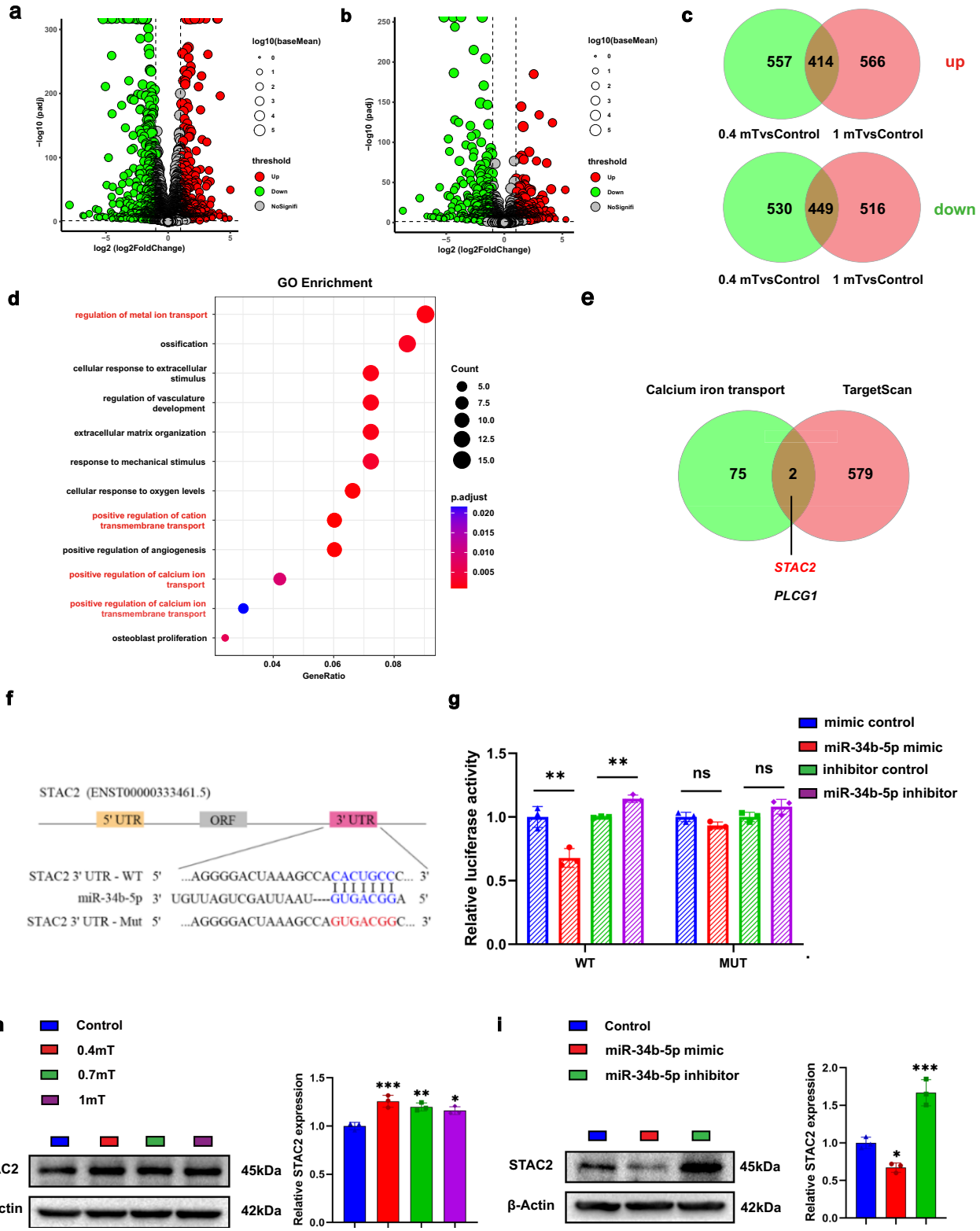

Fig. 6 | miR-34b-5p modulated *STAC2* expression. a Volcano plot depicting the differentially expressed mRNAs in BMSCs after treatment with 0.4 mT SEMFs. **b** Volcano plot depicting the differentially expressed mRNAs in BMSCs after treatment with 1 mT SEMFs. **c** Venn diagram depicting the number of commonly upregulated and downregulated mRNAs in the 0.4 mT and 1 mT groups. **d** Gene Ontology (GO) enrichment analysis of the commonly differentially expressed RNAs in the 0.4 mT and 1 mT groups. **e** Venn diagram showing the intersection between calcium ion transport-related genes from the GO database and the predicted target genes of miR-34b-5p from the TargetScan database. **f** potential binding sites between miR-34b-5p and *STAC2* were predicted using the RNAInter web tool. **g** The interaction between miR-34b-5p and *STAC2* was identified by dual-luciferase reporter assay. **h** The STAC2 protein levels and quantification were assessed in BMSCs following a 7-day exposure to low-frequency SEMFs (0.4–1 mT). **i** STAC2 protein level and quantification were measured in BMSCs following a 7-day transfection with miR-34b-5p mimic and miR-34b-5p inhibitor. Data represent mean ± SD; N = 3/group; $^{*}p < 0.05$; $^{**}p < 0.01$; $^{***}p < 0.001$; ns, not significant by one-way ANOVA.

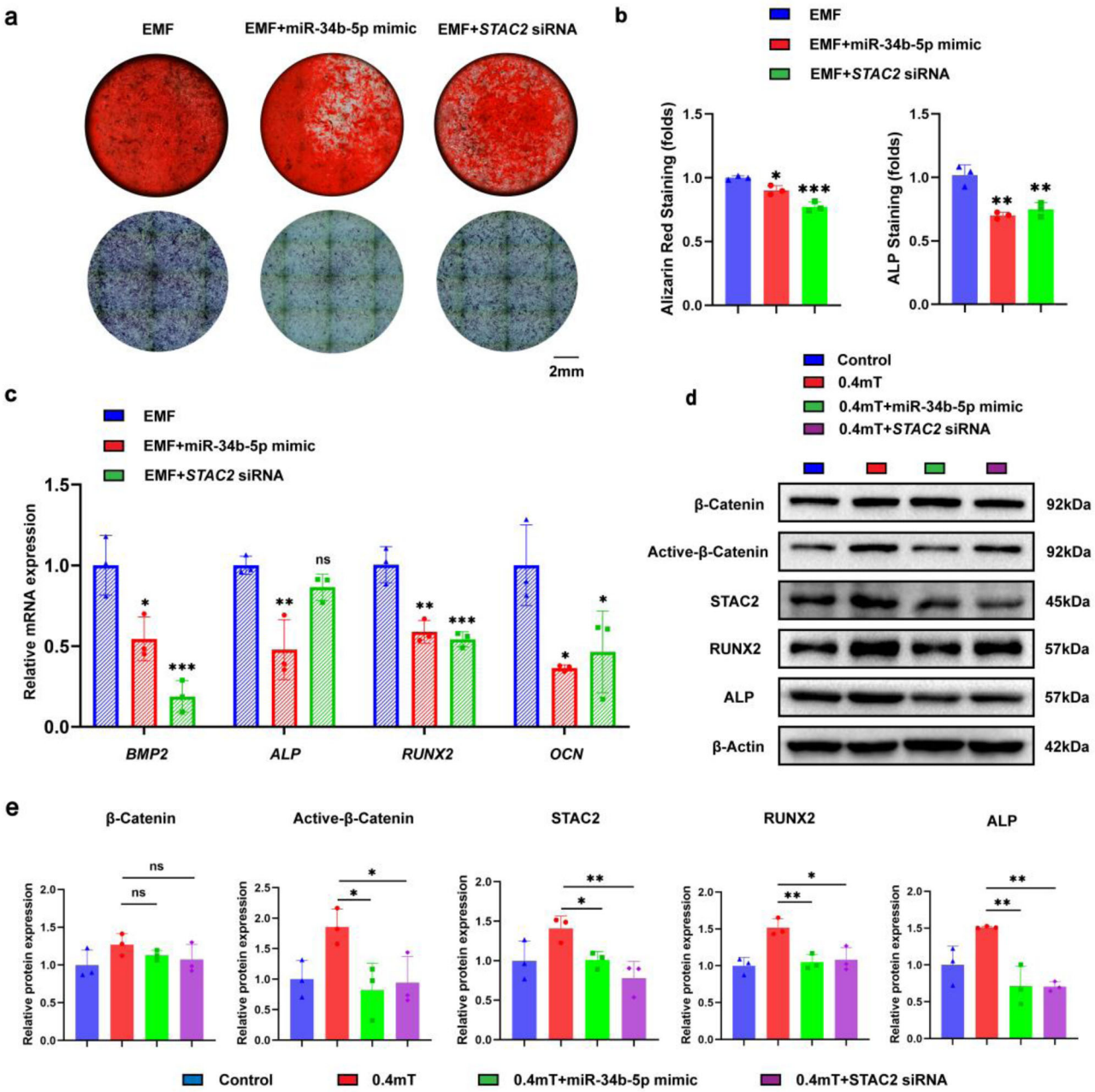

Fig. 7 | Low-frequency SEMFs promoted osteogenic differentiation of BMSCs by regulating miR-34b-5p/*STAC2* axis. a ALP and ARS staining assays of BMSCs transfected with miR-34b-5p mimic or *STAC2* siRNA under low-frequency SEMFs stimulation. **b** Semi-quantitative analyses of ALP and ARS staining intensities. The quantitative analyses of staining intensities were normalized based on changes in cell number resulting from the modulation of miR-34b-5p activity. **c** The mRNA expression levels of *BMP2*, *ALP*, *RUNX2*, and *OCN* after transfection of miR-34b-5p mimic and *STAC2* siRNA under 7-day low-frequency SEMFs stimulation. **d** Westen blot results showing the osteogenic makers (β-catenin, Active-β-catenin, RUNX2, and ALP) with transfection of miR-34b-5p mimic or *STAC2* siRNA under 7-day low-frequency SEMFs stimulation. **e** Quantitative analysis of osteogenic protein and STAC2 expression. Data represent mean ± SD; N = 3/group; $^{*}p < 0.05$; $^{**}p < 0.01$; $^{***}p < 0.001$; ns, not significant by one-way ANOVA.

translation of certain mRNA, thereby maintaining bone homeostasis[43]. Abu-Laban et al. elucidated the osteogenic effects of combining miR-21 and miR-148b mimic in human adipose-derived stem cells[44]. Another study discovered that miR-7-5p increases the expression of RUNX2, ALP, COL1, and OCN by specifically targeting a key regulator of osteogenic differentiation[45]. Notably, miRNAs often act as negative regulators and downregulate during osteogenic induction. Inhibiting miR-29b aims at COL1 and enhance osteogenic differentiation of BMSCs by increasing extracellular matrix[46]. EMF may function as a regulator of miRNAs in BMSCs[21,22]. The up-regulated miR-26a and miR-29b promote osteogenic differentiation of BMSCs when exposed to PEMF stimulation[21]. In addition, increased miR-1260a enhances angiogenesis and osteogenesis under the combined stimulation of magnetic nanoparticles and a static magnetic field[22]. To date, SEMF regulation of miRNAs in stem cells has not been reported. In this study, a total of 98 miRNAs were identified as differentially expressed in response to 0.4 mT SEMFs stimulation, while 86 miRNAs exhibited significant changes following 1 mT SEMFs intervention. Subsequently, the pivotal regulatory function of miR-34b-5p on osteogenic differentiation was validated among 26 co-differentially expressed miRNAs. Our findings provide a preliminary list of miRNAs that are regulated by SEMFs in BMSCs and offer potential targets for subsequent studies.

Calcium ions and calcium channels play a pivotal role in the potential mechanism of EMFs treatment[13]. Previous studies have demonstrated that EMFs activate calcium ion channels, result in calcium influx, and modulate the intracellular calcium pools, thereby inducing calcium oscillations[13]. Consequently, emerging studies have focused on the effects of EMFs-mediated calcium oscillations on the osteogenic differentiation of BMSCs[32,47]. Sequencing analysis in the present study demonstrated similar results, with an increase in calcium ion transport occurring after stimulation with SEMFs. Combined with a library of putative target genes for miR-34b-5p, we identified STAC2, a novel voltage-gated calcium channel protein[48], involved in SEMFs-induced activation of calcium channel. Although STAC2 is predominantly expressed in the nervous system, recent studies have indicated its increased expression in RANKL-induced osteoclasts[49]. Furthermore, it has been shown that STAC2 modulate RANK signaling complex, thereby inhibiting the associated inflammation pathways and osteoclast differentiation[50]. However, the relationship between STAC2 and osteogenesis has not been reported. In the present study, we identified elevated STAC2 expression following SEMFs stimulation. The elevated early osteogenic markers (RUNX2, ALP, Fig. 7) induced by SEMFs underwent a significant downregulation after transfection with miR-34b-5p mimic and *STAC2* siRNAs, suggesting that the downstream calcium iron transport activated by miR-34b-5p/*STAC2* axis mainly regulate early osteogenic differentiation of BMSCs. This result is similar to the early promotion of BMSCs osteogenic differentiation by TRPV4 (a calcium channel)[51]. Overall, increased calcium transport induced by miR-34b-5p/*STAC2* is one of the important mechanisms by which SEMFs affect the fate of BMSCs. However, the specific molecular function of STAC2 in this process still needs to be further investigated.

Conclusion

Low-frequency SEMFs effectively promoted osteogenic differentiation and significantly affected the miRNA expression levels in BMSCs. Specifically, the expression of miR-34b-5p decreased under SEMF stimulation, subsequently increasing *STAC2* level. Targeting the miR-34b-5p/*STAC2* axis effectively modulated SEMF-induced osteogenic activity. The miR-34b-5p/*STAC2* axis regulated by SEMFs may become a possible therapeutic target for osteoporosis.

Materials and methods

EMF device

The EMF generator, designed by the Naval Engineering University (Wuhan, China), consists of a waveform generator, an amplifier, Helmholtz coils, and an oscilloscope. This device is capable of producing SEMFs with adjustable frequencies ranging from 1 to 100 Hz and magnetic field intensities from 0 to 4 mT. During operation, the electromagnetic signals generated by the waveform generator are amplified before being output to the Helmholtz coils, which are wound with 0.8-mm coated copper wire. The Helmholtz coils are placed inside an incubator maintained at a constant temperature of 37 °C and 5% CO_2, ensuring optimal experimental conditions for research and testing purposes.

BMSCs harvest and culture

BMSCs were harvested from 8-week-old male Sprague Dawley (SD) rats. The experimental procedures have been reviewed and approved by Ethics Committee of Experimental Animal Center of Huazhong University of Science and Technology (No. 3091, Wuhan, China). We have complied with all relevant ethical regulations for animal use. After the rats were sacrificed, their femurs and tibiae were removed under sterile conditions and immersed in sterile phosphate-buffered saline (PBS; Boster Bio Tech, Wuhan, China). The epiphyses were then removed, and each bone marrow cavity was thoroughly washed with Dulbecco's modified Eagle medium (DMEM)/F12 culture medium containing 10% fetal bovine serum (FBS; Gibco, Grand Island, USA), 100 units/mL penicillin and 100 μg/mL streptomycin (Gibco). The cells were resuspended in the above complete medium and cultured in an incubator (37 °C, 5% CO_2, and 100% humidity) for subsequent experiments. The culture medium was changed every other day.

Table 1 | Rat primer sequences for RT-PCR

Gene		Primers (5′-3′)
β-Actin	Forward	GGCTGTATTCCCCTCCATCG
	Reverse	CCAGTTGGTAACAATGCCATGT
ALP	Forward	CAAGGACCAACTACAACCA
	Reverse	AGGGAAGGGTCAGTCAGGTT
BMP-2	Forward	AACGAGAAAAGCGTCAAGCC
	Reverse	CCAGTCATTCCACCCCACA
OCN	Forward	GGAGGGCAGTAAGGTGGTGA
	Reverse	GAAGCCAATGTGGTCCGC
OPN	Forward	CAAGGACCAACTACAACCA
	Reverse	GGAGACAGGAGGCAAGG
RUNX2	Forward	CTACTCTGCCGAGCTACGAAAT
	Reverse	TCTGTCTGTGCCTTCTTGGTTC

BMSCs passage and stimulation

When the BMSCs reached about 90% confluence, they were detached using 0.25% Trypsin/EDTA (Gibco, Grand Island, USA) and passaged at a ratio of 1:3. The cells from passage 3 were counted, and then 2.5–3 × 10^5 cells were seeded into 6-well plate. After 24 h, the culture medium was replaced with osteogenic medium (OM; Cyagen, Shanghai, China). The specific arrangement of SEMF exposure on cells is shown in Fig. 1a. Briefly, the cells were individually exposed to SEMFs stimulation at a fixed frequency (15 Hz) and different intensities (0.4 mT, 0.7 mT, and 1 mT) for 7 or 14 days, 4 h per day. On the 7th day, RNA and protein expression levels were detected, and ALP staining was performed. On the 14th day, ARS staining was conducted.

RNA extraction and real time-quantitative polymerase chain reaction (RT-qPCR)

Total RNA was extracted using E.Z.N.A.® total RNA Kit I (Omega Bio-Tek, USA). The extracted RNA was then assessed for concentration and purity using a microplate reader (Bio-Tek USA). Subsequently, 1 μg RNA was transcribed to cDNA using a one-step RT-qPCR kit (Vazyme, China). The cDNA, SYBR Green Master mix and primers were mixed proportionally, amplified, and measured in RT-qPCR detection device. Relative mRNA levels were normalized for quantification compared with *β-Actin* levels. The primer sequences used in the experiment were listed in Table 1.

Alkaline phosphatase (ALP) and Alizarin Red S (ARS) staining assay

BMSCs were seeded into 24-well plates for ALP staining after 7-day SEMF stimulation while ARS staining was performed after 14 days of intervention. The cells were fixed with 4% paraformaldehyde (Sigma, USA) for 30 min and then washed with PBS. Subsequently, each well was stained with 350 μL of ALP or ARS staining solution for 10 min. After three rinses with PBS, the stained cells were observed and photographed under a fluorescence microscope. Quantitative analysis of the staining intensity was carried out using Image J software.

Western blotting analysis

Cultured BMSCs were lysed with enhanced RIPA lysis buffer (Boster) containing 1% EDTA, protease, and phosphatase inhibitor cocktails. Following the determination of the protein concentration of the cell lysates, equal amounts of samples were separated by 10% SDS-PAGE and the protein bands were then transferred to polyvinylidene fluoride (PVDF; Millipore, USA) membranes. After being blocked with 5% bovine serum albumin (BSA; BioFroxx, Germany) for 1 h, the membrane bands were

Table 2 | Sequences of miR-34b-5p mimic, miR-34b-5p inhibitor and *STAC2* siRNA

Gene	Sequences (5′-3′)
rno-miR-34b-5p mimic	UUCAAGUAAUCCAGGAUAGGCU
rno-miR-34b-5p inhibitor	AGCCUAUCCUGGAUUACUUGAA
STAC2 siRNA	GAAACCAAGCUCCAGCGAUUUTT

incubated at 4 °C overnight with their corresponding primary antibodies (anti-β-catenin, anti-Active-β-catenin, anti-OPN, anti-RUNX2, anti-ALP, anti-STAC2 and anti-β-Actin, Cell Signaling Technology, USA). The blots were subsequently incubated with secondary antibodies (Boster) for 1 h the next day. The target protein bands were visualized using Image Lab System (Bio-Rad, USA). Relative target protein levels were normalized for quantification compared with β-Actin.

Cell transfection

Approximal 2×10^5 BMSCs were seeded into 6-well plates. When the cell confluences reached around 80%, Lipofectamine 3000 reagent (Invitrogen, USA) was used for transfection. In each well, Opti-MEM (250 μL) and lipofectamine 3000 (5 μL) were added along with either miR-34b-5p mimic or inhibitor (20 μM, 50 μM, and 100 μM, Tsingke, China) or *STAC2* siRNA (50 Mm, Tsingke). The cells were then incubated for 48 h. In order to maintain intracellular levels of miR-34b-5p and *STAC2* during the long culture period of BMSCs (7 or 14 days), cell transfection was performed every 4 days. The transfection efficiency was visualized using fluorescence microscopy. The miRNA sequences used in the study were listed in Table 2.

miRNA sequencing

The total RNA was extracted from the samples using the miRNeasy Micro Kit (Qiagen, Germany). Subsequently, miRNAs were extracted and purified using the miRNA isolation kit (Sigma). Next, the complemental DNA (cDNA) library was prepared following the manufacturer's instructions of the RNA Library Kit (Vazyme, China). The constructed library was processed on the Illumina HiSeq 4000 platform and low-quality reads were removed using Skewer 0.2.2. Principal component analysis (PCA) was employed to assess the transcriptome differences between each group. Differentially expressed miRNAs (DE-miRNAs) were determined based on the criteria of False Discovery Rate (FDR) < 0.05[52]. The cutoff for identifying DE-miRNAs was set at an adjusted $p < 0.05$ and a $|\log_2$ fold change $(\log_2 FC)| \geq 0.585$. TargetScan database (http://www.targetscan.org/mamm_31/) was used to predict the target genes of miR-34b-5p.

RNA sequencing and bioinformatic analysis

The total RNA was extracted as described above. Subsequently, 500 ng of RNA was utilized to construct cDNA libraries, which underwent high-throughput sequencing on the Illumina HiSeq 4000 platform. Quality assessment of the raw reads was performed using FastQC (v0.10.1). Following this, the acquired data underwent preprocessing to remove low-quality reads, quantify gene expression, and compare against a reference genome. The screening criteria of differentially expressed genes (DEGs) was set at an adjusted p-value of less than 0.05 and $|\log_2 FC| \geq 1$. The pathways associated with calcium channels were investigated using Gene Ontology (GO) database. Kyoto Encyclopedia of Genes and Genomes (KEGG) enrichment analysis was conducted with R package (v3.11).

EdU assay

EdU assay (beyotime, China) was used for assessing cell proliferation. BMSCs were seeded in a 96-well plate and incubated with 100 μL EdU (10 μM) for 2 h. After fixed with 4% paraformaldehyde for 20 min and permeabilized with 3% Triton-X100 for 15 min, the cells were incubated with a mixed staining solution according to the manufacturer's protocol for 1 h. Hoechest 33342 was added to incubate for 10 min. The stained cells were visualized under a fluorescence microscope (Nikon, Japan).

Luciferase reporter assay

TargetScan and RNAInter web were used to analyze the potential binding sites between miR-34b-5p and *STAC2*. The wild-type (WT) and corresponding mutant sequences of *STAC2* were cloned into the pMIR-report vector. BMSCs were then seeded into 24-well plates and co-transfected with either the WT or mutant (MUT) plasmids, along with miR-34b-5p mimic, miR-34b-5p inhibitor, or their respective negative controls. Following 48 h of culture, cells were lysed, and the luciferase activity was measured using the Luciferase Reporter System (Promega, USA).

OVX rat model

In this study, all 12-week-old female SD rats were obtained from SJA Laboratory Animal Company (Certificate No. SCXK, Hunan, 2021-001, China). The methods were performed in accordance with relevant guidelines and regulations and approved by the Ethics Committee of Experimental Animal Center of Huazhong University of Science and Technology (No. 3091, Wuhan, China). A total of 18 rats were randomly divided into three groups (n = 6 per group). The groups were designated as follows: sham, OVX, and OVX + miR-34b-5p inhibitor. In the sham-operated group, only the adipose tissue surrounding the ovaries was removed. Bilateral ovariectomy was performed under anesthesia in both OVX control and OVX + miR-34b inhibitor groups. After a 2-week recovery period, a 2 mm diameter hole was drilled in the proximal femur of each rat. In the sham and OVX group, rats were intramedullary injected 5 μL of normal saline, while rats in OVX+miR-34b-5p inhibitor group received injections of 5 μL miR-34b-5p inhibitor solution (20 mmol/L) every 2 weeks. The holes were sealed with bone wax following each injection. After 10 weeks of injections, all rats were euthanized, and their femurs were harvested.

Micro-CT scanning

The collected femurs were fixed using 4% paraformaldehyde solution for 24 h. Subsequently, the microstructure of the bone was analyzed using the Viva CT 40 microcomputed tomography (micro-CT) system (Scanco, Switzerland). Our analysis primarily focused on the cancellous bone, and several trabecular morphometry parameters, including trabecular bone volume per tissue volume (BV/TV), trabecular number (TB.N), trabecular thickness (TB.Th), and trabecular separation (Tb.Sp).

Hematoxylin and Eosin (H&E) staining

The femur samples were fixed and decalcified in 10% EDTA solution for 4 weeks and embedded in paraffin. Following embedding, they were cut into sections and deparaffinized using xylene. Subsequently, the sections were incubated with hematoxylin for 5 min, followed by washing with acid ethanol. Next, the sections were incubated with 0.5% eosin, dehydrated stepwise, and blocked using Permount (Absin, China). The sections were observed and photographed under a light microscope (Olympus, Japan).

Masson staining assay

The Masson staining assay was conducted using the Trichrome Stain Kit (Sigma) following the provided protocol. After deparaffinization with xylene, the sections were immersed in Bouin's Solution overnight. The slices were sequentially incubated with Hematoxylin Solution, Biebrich Scarlet-Acid Fuchin Solution, and Phosphotungstic/Phosphomolybdic Acid Solution for 5 min each. Then, the sections underwent staining with Aniline Blue solution for 8 min, followed by dehydration. Finally, the slides were blocked with a drop of Permount and observed using a light microscope.

Statistics and reproducibility

All experimental data were analyzed using GraphPad Prism V.8 software (GraphPad Software, USA), and the results were shown as mean ± standard deviation (SD). Animal experiments and cell experiments were independently replicated six times and three times, respectively. The differences among multiple groups were analyzed using one-way analysis of variance (ANOVA). A value of $p < 0.05$ was considered statistically significant.

Reporting summary

Further information on research design is available in the Nature Portfolio Reporting Summary linked to this article.

Data availability

The data that support the findings of this study are available from the corresponding author upon reasonable request or Supplementary information. All source data for the graphs are shown in the Supplementary Data 5. The unedited blots were presented in Supplementary Fig. 2. The sequencing data have been uploaded to the NCBI Sequence Read Archive (SRA) with an SRA accession code: SRP527101.

Received: 12 October 2023; Accepted: 9 September 2024;
Published online: 16 September 2024

References

1. Ensrud, K. E. & Crandall, C. J. Osteoporosis. *Ann. Intern. Med.* **177**, Itc1–itc16 (2024).
2. Szulc, P. Bone turnover: biology and assessment tools. *Best. Pract. Res. Clin. Endocrinol. Metab.* **32**, 725–738 (2018).
3. Walker, M. D. & Shane, E. Postmenopausal osteoporosis. *N. Engl. J. Med.* **389**, 1979–1991 (2023).
4. Dong, Y. et al. A clinical-stage Nrf2 activator suppresses osteoclast differentiation via the iron-ornithine axis. *Cell Metab.* **36**, 1679–1695.e6 (2024).
5. Tan, F. et al. Clinical applications of stem cell-derived exosomes. *Signal Transduct. Target. Ther.* **9**, 17 (2024).
6. Bianco, P. "Mesenchymal" stem cells. *Annu. Rev. Cell Dev. Biol.* **30**, 677–704 (2014).
7. Wu, T. et al. METTL3-m(6) A methylase regulates the osteogenic potential of bone marrow mesenchymal stem cells in osteoporotic rats via the Wnt signalling pathway. *Cell Prolif.* **55**, e13234 (2022).
8. Chen, L. et al. KIAA1199 deficiency enhances skeletal stem cell differentiation to osteoblasts and promotes bone regeneration. *Nat. Commun.* **14**, 2016 (2023).
9. Kim, H. K. et al. Bone-forming peptide-2 derived from BMP-7 enhances osteoblast differentiation from multipotent bone marrow stromal cells and bone formation. *Exp. Mol. Med.* **49**, e328 (2017).
10. He, W. F. et al. The interdependent relationship between the nitric oxide signaling pathway and primary cilia in pulse electromagnetic field-stimulated osteoblastic differentiation. *FASEB J.* **36**, e22376 (2022).
11. Tu, C., Xiao, Y., Ma, Y., Wu, H. & Song, M. The legacy effects of electromagnetic fields on bone marrow mesenchymal stem cell self-renewal and multiple differentiation potential. *Stem Cell Res. Ther.* **9**, 215 (2018).
12. Wang, M. et al. Pulsed electromagnetic field enhances healing of a meniscal tear and mitigates posttraumatic osteoarthritis in a rat model. *Am. J. Sports Med.* **50**, 2722–2732 (2022).
13. Ma, T., Ding, Q., Liu, C. & Wu, H. Electromagnetic fields regulate calcium-mediated cell fate of stem cells: osteogenesis, chondrogenesis and apoptosis. *Stem Cell Res. Ther.* **14**, 133 (2023).
14. Ross, C. L. et al. The effect of low-frequency electromagnetic field on human bone marrow stem/progenitor cell differentiation. *Stem Cell Res.* **15**, 96–108 (2015).
15. Tu, C. et al. Effects of electromagnetic fields treatment on rat critical-sized calvarial defects with a 3D-printed composite scaffold. *Stem Cell Res. Ther.* **11**, 433 (2020).
16. Li, W. et al. Low-frequency electromagnetic fields combined with tissue engineering techniques accelerate intervertebral fusion. *Stem Cell Res. Ther.* **12**, 143 (2021).
17. Hu, X. et al. Electromagnetic field-mediated chitosan/gelatin/nano-hydroxyapatite and bone-derived scaffolds regulate the osteoblastic and chondrogenic phenotypes of adipose-derived stem cells to construct osteochondral tissue engineering niche in vitro. *Int. J. Biol. Macromol.* **258**, 128829 (2024).
18. Liao, Y. H. et al. Osteogenic differentiation of adipose-derived stem cells and calvarial defect repair using baculovirus-mediated co-expression of BMP-2 and miR-148b. *Biomaterials* **35**, 4901–4910 (2014).
19. Bartel, D. P. MicroRNAs: target recognition and regulatory functions. *Cell* **136**, 215–233 (2009).
20. Yan, J. et al. Effects of miR-26a on osteogenic differentiation of bone marrow mesenchymal stem cells by a mesoporous silica nanoparticle-PEI-peptide system. *Int. J. Nanomed.* **15**, 497–511 (2020).
21. De Mattei, M. et al. Pulsed electromagnetic fields modulate miRNAs during osteogenic differentiation of bone mesenchymal stem cells: a possible role in the osteogenic-angiogenic coupling. *Stem Cell Rev. Rep.* **16**, 1005–1012 (2020).
22. Wu, D. et al. Bone mesenchymal stem cells stimulation by magnetic nanoparticles and a static magnetic field: release of exosomal miR-1260a improves osteogenesis and angiogenesis. *J. Nanobiotechnology* **19**, 209 (2021).
23. Aalami Zavareh, F., Abdi, S. & Entezari, M. Up-regulation of miR-144 and miR-375 in the human gastric cancer cell line following the exposure to extremely low-frequency electromagnetic fields. *Int. J. Radiat. Biol.* **97**, 1324–1332 (2021).
24. Sharma, S. et al. Ca(2+) and CACNA1H mediate targeted suppression of breast cancer brain metastasis by AM RF EMF. *EBioMedicine* **44**, 194–208 (2019).
25. Chen, Y. et al. Exposure to 16 Hz pulsed electromagnetic fields protect the structural integrity of primary cilia and associated TGF-β signaling in osteoprogenitor cells harmed by cigarette smoke. *Int. J. Mol. Sci.* **22**, 7036 (2021).
26. Park, J. E. et al. Electromagnetic fields induce neural differentiation of human bone marrow derived mesenchymal stem cells via ROS mediated EGFR activation. *Neurochem. Int.* **62**, 418–424 (2013).
27. Cheng, G. et al. Sinusoidal electromagnetic field stimulates rat osteoblast differentiation and maturation via activation of NO-cGMP-PKG pathway. *Nitric oxide* **25**, 316–325 (2011).
28. Mayourian, J. et al. Exosomal microRNA-21-5p mediates mesenchymal stem cell paracrine effects on human cardiac tissue contractility. *Circ. Res.* **122**, 933–944 (2018).
29. Liu, F. et al. MicroRNA-27a controls the intracellular survival of Mycobacterium tuberculosis by regulating calcium-associated autophagy. *Nat. Commun.* **9**, 4295 (2018).
30. Zhang, Y. et al. Electromagnetic field treatment increases purinergic receptor P2X7 expression and activates its downstream Akt/GSK3β/β-catenin axis in mesenchymal stem cells under osteogenic induction. *Stem Cell Res. Ther.* **10**, 407 (2019).
31. Jimenez, H. et al. Tumour-specific amplitude-modulated radiofrequency electromagnetic fields induce differentiation of hepatocellular carcinoma via targeting Ca(v)3.2 T-type voltage-gated calcium channels and Ca(2+) influx. *EBioMedicine* **44**, 209–224 (2019).
32. Zhang, Y. et al. Extremely low frequency electromagnetic fields promote mesenchymal stem cell migration by increasing intracellular Ca(2+) and activating the FAK/Rho GTPases signaling pathways in vitro. *Stem Cell Res. Ther.* **9**, 143 (2018).
33. Barati, M. et al. Necroptosis triggered by ROS accumulation and Ca(2+) overload, partly explains the inflammatory responses and anti-cancer effects associated with 1Hz, 100 mT ELF-MF in vivo. *Free Radic. Biol. Med.* **169**, 84–98 (2021).
34. Yan, Z. et al. High-specificity protection against radiation-induced bone loss by a pulsed electromagnetic field. *Sci. Adv.* **8**, eabq0222 (2022).

35. Ferroni, L. et al. Pulsed electromagnetic fields increase osteogenetic commitment of MSCs via the mTOR pathway in TNF-α mediated inflammatory conditions: an in-vitro study. *Sci. Rep.* **8**, 5108 (2018).
36. Sun, L. Y., Hsieh, D. K., Lin, P. C., Chiu, H. T. & Chiou, T. W. Pulsed electromagnetic fields accelerate proliferation and osteogenic gene expression in human bone marrow mesenchymal stem cells during osteogenic differentiation. *Bioelectromagnetics* **31**, 209–219 (2010).
37. Poh, P. S. P. et al. Osteogenic effect and cell signaling activation of extremely low-frequency pulsed electromagnetic fields in adipose-derived mesenchymal stromal cells. *Stem Cells Int.* **2018**, 5402853 (2018).
38. Jansen, J. H. et al. Stimulation of osteogenic differentiation in human osteoprogenitor cells by pulsed electromagnetic fields: an in vitro study. *BMC Musculoskelet. Disord.* **11**, 188 (2010).
39. Chen, J. et al. The combinatory effect of sinusoidal electromagnetic field and VEGF promotes osteogenesis and angiogenesis of mesenchymal stem cell-laden PCL/HA implants in a rat subcritical cranial defect. *Stem Cell Res. Ther.* **10**, 379 (2019).
40. Ledda, M. et al. Nonpulsed sinusoidal electromagnetic fields as a noninvasive strategy in bone repair: the effect on human mesenchymal stem cell osteogenic differentiation. *Tissue Eng. Part C. Methods* **21**, 207–217 (2015).
41. Liu, C. et al. Effect of 1 mT sinusoidal electromagnetic fields on proliferation and osteogenic differentiation of rat bone marrow mesenchymal stromal cells. *Bioelectromagnetics* **34**, 453–464 (2013).
42. Zhou, J. et al. Sinusoidal electromagnetic fields increase peak bone mass in rats by activating Wnt10b/β-catenin in primary cilia of osteoblasts. *J. Bone Miner. Res.* **34**, 1336–1351 (2019).
43. Lian, J. B. et al. MicroRNA control of bone formation and homeostasis. *Nat. Rev. Endocrinol.* **8**, 212–227 (2012).
44. Abu-Laban, M. et al. Combinatorial delivery of miRNA-nanoparticle conjugates in human adipose stem cells for amplified osteogenesis. *Small* **15**, e1902864 (2019).
45. Tang, Z. et al. Inhibition of CRY2 by STAT3/miRNA-7-5p promotes osteoblast differentiation through upregulation of CLOCK/BMAL1/P300 expression. *Mol. Ther. Nucleic Acids* **19**, 865–876 (2020).
46. Li, Z. et al. Correction: biological functions of miR-29b contribute to positive regulation of osteoblast differentiation. *J. Biol. Chem.* **294**, 10018 (2019).
47. Wu, S., Yu, Q., Lai, A. & Tian, J. Pulsed electromagnetic field induces Ca(2+)-dependent osteoblastogenesis in C3H10T1/2 mesenchymal cells through the Wnt-Ca(2+)/Wnt-β-catenin signaling pathway. *Biochem. Biophys. Res. Commun.* **503**, 715–721 (2018).
48. Jeong, E., Choi, H. K., Park, J. H. & Lee, S. Y. STAC2 negatively regulates osteoclast formation by targeting the RANK signaling complex. *Cell Death Differ.* **25**, 1364–1374 (2018).
49. Polster, A. et al. Stac proteins suppress Ca(2+)-dependent inactivation of neuronal l-type Ca(2+) channels. *J. Neurosci.* **38**, 9215–9227 (2018).
50. Zhao, X. et al. The histone methyltransferase ASH1L protects against bone loss by inhibiting osteoclastogenesis. *Cell Death Differ.* **31**, 605–617 (2024).
51. Hu, K., Sun, H., Gui, B. & Sui, C. TRPV4 functions in flow shear stress induced early osteogenic differentiation of human bone marrow mesenchymal stem cells. *Biomed. Pharmacother.* **91**, 841–848 (2017).
52. Love, M. I., Huber, W. & Anders, S. Moderated estimation of fold change and dispersion for RNA-seq data with DESeq2. *Genome Biol.* **15**, 550 (2014).

Acknowledgements

This research was supported by the Natural Science Foundation of the Science and Technology Department of Hubei Province (2022CFB274) and the Nation Pulsed High Magnetic Field Center of Huazhong University of Science and Technology (WHMFC202211). The authors appreciated the Experimental Medicine Research Center of Tongji Hospital, Huazhong University of Science and Technology, for providing the experimental instruments and equipment.

Author contributions

All authors listed have made corresponding and intellectual contribution to this work and approved it for publication. Xuan Fang: data curation, cell experiments, writing and editing manuscript; Changyu Liu: experimental design, animal study, writing original draft; Kang Wei and Zixing Shu: cell and molecular experiments; Zihao Zhang and Yi Zou: bioinformatic analysis; Qing Ding, Shaoze Jing and Hao Li: animal experiments; Weigang Li and Tianqi Wang: cell and molecular experiment; Hua Wu: experimental design; Chaoxu Liu: project conceptualization and administration; Tian Ma: funding acquisition, cell and molecular experiments, project conceptualization and supervision.

Competing interests

The authors declare no competing interests.

Additional information

Supplementary information The online version contains supplementary material available at https://doi.org/10.1038/s42003-024-06866-3.

Correspondence and requests for materials should be addressed to Chaoxu Liu or Tian Ma.

Peer review information *Communications Biology* thanks Jian Zhou, Yadav Wagley, and the other, anonymous, reviewer(s) for their contribution to the peer review of this work. Primary Handling Editors: Martina Rauner and David Favero.